MICROMECHANICS OF COMPOSITE ANISOGRID STRUCTURES

G. Totaro[a*], F. De Nicola[a], A. Grilli[b], A. Ferrigno[a], P. Caramuta[a]

[a]*Advanced Materials and Technologies, CIRA - Italian Aerospace Research Center, Via Maiorise, 81043, Capua, Italy.*
[b]*IMAST - Technological District on Engineering of Polymeric and Composite Materials and Structures, Piazzale Enrico Fermi 1, 80055, Portici, Italy.*
**g.totaro@cira.it*

Keywords: anisogrid, fiber fraction, microstructure, rubber tool.

Abstract
It is well-known that the typical fiber volumetric fraction in composite anisogrid lattice structures ranges around 30-35%. This fact is intrinsic to the manufacturing process which involves continuous fiber tows forming a regular system of interlaced unidirectional ribs. This low fiber fraction is reflected in the basic mechanical properties which drive the optimal design, namely, the longitudinal compressive stiffness and strength of ribs. In this research activity, the possibility to modify the typical fiber content in the ribs is preliminarily explored with the aid of a lattice anisogrid panel, in which possible deviations from the baseline manufacturing process are tested at the same time. The baseline process here is based on the deposition of dry fiber tows, rubber tooling, and resin infusion.

1. Introduction

Interlaced fiber tows, which provide the basis for the continuous deposition process of composite lattice structures, involve a decrease of fiber volumetric fraction passing from the nodal regions to the ribs. An immediate consequence of this fact is given by the reduction of the longitudinal stiffness of ribs, as represented by the simple rule of mixture. Another similar consequence occurs for the longitudinal coefficient of thermal expansion (CTE), which is even more affected by the low fiber content. Less evident is the effect of the fiber fraction on the compressive strength of helical ribs. As a general trend, the fiber fraction and specific stiffness maximization does not correspond to the maximization of the specific compressive strength. However, original Russian anisogrids [1], which are based on the wet filament winding process, demonstrate that the relatively low longitudinal compressive stiffness and strength of ribs are still sufficient to design the lightest heavily-loaded structures in the field of space launchers.
Dry robotic filament winding and resin infusion reveal an interesting option for the manufacturing of low-cost and efficient composite lattice structures, as shown in the prototypical interstage demonstrator represented in [2].
In many design cases, minimum mass solutions of anisogrids are associated with global buckling failure mechanism, whereas compressive failure of ribs still preserves some positive margins of safety. This fact may especially occur when stiffness requirements largely overcomes the stiffness associated with the minimum mass solution, for example, in case of stiff and thermally stable lattice panels and shells, in which mechanical loads are relatively

low. In this case, it could be beneficial to increase the fiber volumetric fraction and stiffness of ribs, even if a probable compressive strength reduction can be expected.
Ideally, the optimal fiber fraction in the ribs should be addressed according to the specific application, and controlled in the manufacturing process. With this aim, preliminary tests were realized based on specimens cut from a flat anisogrid lattice panel, in which two main regions were considered: the right side, for the baseline manufacturing process, and the left side for some modifications of the baseline process (Figure 1). Experimental results were obtained for the axial compression of single units, flexural lateral stiffness and strength of helical ribs, and for the longitudinal coefficient of thermal expansion. Clearly, the idea was just to catch the tendency of some mechanical properties, being the number of samples extracted from the test-article necessarily limited.

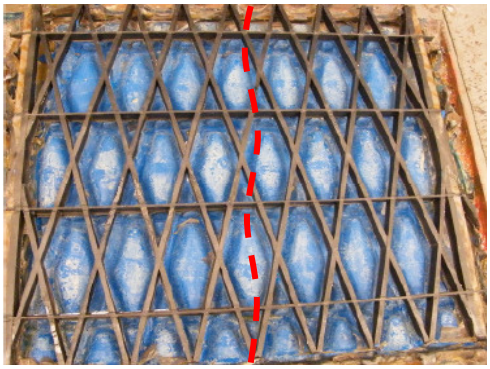

Figure 1. Anisogrid test-article with alternative (left part) and baseline (right part) microstructure.

2. Baseline process and rib microstructure

Here the baseline process and microstructure consists in dry interlaced fiber tows laid down in helical and hoop rubber grooves having certain nominal widths, b_h and b_c, respectively, and the same nominal thickness, H. After the complete deposition of tows, the process is completed with resin infusion under vacuum bag and oven cure. This process is basically the same as applied for the manufacturing of the interstage prototype [2]. The nominal value of the fiber volumetric fraction in the ribs, V_{fB}, can be readily anticipated as,

$$V_{fB} = \frac{nN_t k}{A_n}\left(\frac{\pi D^2}{4}\right) \tag{1}$$

in which k is the number of filaments for each tow, N_t is the number of tow passages in the groove for each layer, n is the number of layers, D is average fiber diameter, and A_n is the cross-section of the respective grooves (hoop or helical), or the nominal rib width. In this case, the adopted carbon fiber tow was IM7 whose characteristics are: D = 5.2 μm, k = 12e3, whereas the nominal helical rib width is b_h = 6.0 mm, the nominal hoop width is b_c = 3.0 mm, and the rib thickness is H = 18 mm. Moreover, N_t = 4 for helical ribs and N_t = 2 for hoop ribs were adopted. Considering that n = 32 layers were laid down in the grooves, we find from Eq.(1) that the nominal fiber volumetric fraction is the same for hoop and helical ribs, that is, V_{fB} = 30.2%. Considering this fiber fraction, the nominal longitudinal compression modulus of hoop and helical ribs will be approximated by the simple rule of mixture i.e.,

$$E_B = 0.9V_{fB}E_{tow} \tag{2}$$

which yields E_B = 75 GPa, with the modulus of tow E_{tow} = 276 GPa. In such evaluation, a knock-down factor of 10% was introduced for the compression modulus with respect to tensile modulus (consistently with data shown in many datasheet of general composites). The rule of mixture for the mass density of ribs yields ρ_B = 1333 kg/m^3. An example of the rib baseline microstructure in cross-section is represented in Figure 2, showing at increasing magnification the good compaction of the specimen.

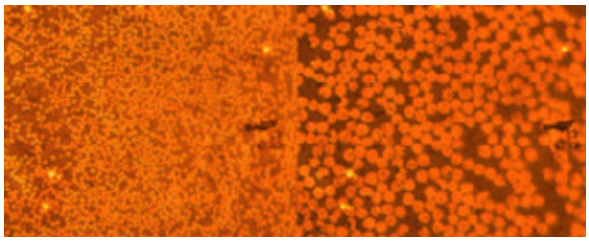

Figure 2. Example of baseline microstructure of ribs at 1100x, 2750x.

3. Reinforced rib microstructure

One of the tested modifications of the baseline microstructure concerns the use of helical ribs reinforced with additional fibers. Such deviation aims at an increase of the fiber content and stiffness and consists in the use of additional pieces of unidirectional dry fabric made of HS carbon fibers. These pieces were cut in shape of the grooves of helical ribs, filling the space between two consecutive nodes and the space through the thickness (which is normally filled by resin). Such pieces were manually placed and regularly alternated with the normal tows of the baseline process (Figure 3).

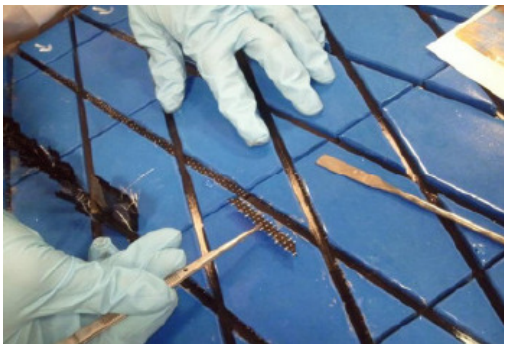

Figure 3. Specimen of UD fabric used to reinforce the helical ribs.

In case of a fabric, the nominal fiber content, V_{fF}, can be evaluated introducing the mass of the dry fabric, m_f, whose microstructure is known,

$$m_f = \rho_f V_{ff} nAt = \gamma An \tag{3}$$

in which V_{ff} is the fiber volumetric fraction of the fabric, n is the number of layers, A is the reference surface, t is the total thickness, ρ_f = 1780 kg/m^3 is the mass density of the carbon fabric, and γ= 290 g/m^2 is the areal weight of the single layer which is normally provided by datasheet. The nominal fiber volumetric fraction of the fabric added in the grooves can be expressed as:

$$V_{fF} = \frac{V_{ff} nAt}{AH} = \frac{n\gamma}{\rho_f H} \tag{4}$$

In the experimental situation, the total number of tows was n_{tow} = 27, and the number of additional pieces of UD fabric was n_{fab} = 28. Such values were determined by practical reasons during the deposition (the thickness of reinforced ribs increased more than expected). Assuming that the pieces of fabric have the same width as the helical groove b_h, we have:

$$V_{fR} = \frac{n_{tow} N_t k}{H b_h} \left(\frac{\pi D^2}{4} \right) + \frac{n_{fab} \gamma}{\rho_f H} \tag{5}$$

which corresponds to the 25.4% of tow and almost the same for the fabric, resulting in a total fiber volumetric fraction in the reinforced ribs equal to V_{fR} = 50.8%. Thus, the nominal compressive modulus will be approximated as,

$$E_R = 0.9 \left[\frac{n_{tow} N_t k}{H b_h} \left(\frac{\pi D^2}{4} \right) E_{tow} + \frac{n_{fab} \gamma}{\rho_f H} E_{fab} \right] \tag{6}$$

which yields E_R = 116 GPa, with the modulus of fabric E_{fab} = 230 GPa. In consideration of Eq. (5), the rule of mixture for the mass density of the reinforced ribs yields ρ_{fR} = 1465 kg/m^3. An example of the microstructure of reinforced rib is shown in cross-section in Figure 4, with an emphasis on the pure resin in correspondence of the red-colored area. In the picture on the right, a magnification allows to distinguish a layer of fabric surrounded by two layers of tow. The different size of carbon fibers, IM7 vs. HS, can be distinguished, too.

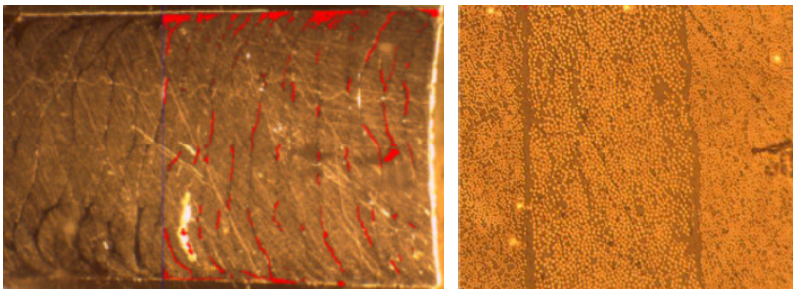

Figure 4. Example of microstructure in reinforced ribs, at cross-section level (left) and at tow/fabric level (right).

4. Rubber tooling, innovative manufacturing approach

Previous experience on the rubber tooling revealed some difficulties in the extraction of the carpet from anisogrids with the skin, also in consideration of the small size of the triangular cells and the high rib thickness. In order to improve both the extraction and reusability of the rubber carpet, a double-carpet approach was attempted for the test-article manufacturing (Figure 5). The carpet is made of a “volumetric part” and a “shape part”. A male mold reproducing the system of ribs was firstly made. In this case, an aluminum mold was adopted, but other expendable and low-cost materials can be clearly used, too. The volumetric part of the carpet was made with a breather and a vacuum bag to pour the liquid rubber and vulcanize in environmental condition. The use of the breather allows to round the edges of the mold, and obtain an adequate shape for the extraction of volumetric part from the geometric part. The geometric part of the carpet - which will be in contact with tows and will determine the final shape of the ribs - was obtained with a second pouring of liquid rubber on the first carpet (which was previously treated with a release spray). Finally, the male mold was finally placed on top of the liquid rubber and pressed. Rubber vulcanization was completed in environmental condition.

Figure 5. Aluminum male mold and vacuum bag (left) for preparation of double-carpet rubber tool: volumetric part (center) and geometric part (right).

It is clear that the specific cure process and rubber tooling will determine the effective final fiber volumetric fraction in the ribs. In fact, measurements with the aid of microscopy and caliper indicated for the baseline process a cross-sectional reduction of about 18% and 35% for helical and hoop ribs, respectively, whereas the reduction of cross-section in reinforced ribs was less relevant. This fact, in light of the cross-section upgrade in Eq.(1), indicates an increase of the actual fiber volumetric fraction in the baseline ribs, that is, 37% and 47% for helical and hoop ribs, respectively. Thus, starting from the same nominal fiber fraction in hoop and helical ribs, we arrive at a rather different final value. This fact is related to different thermal expansion of the rubber blocks in the principal directions, due to the specific rubber material, the shape and size of the blocks, and the cure cycle itself. As a consequence, neglecting the fact that such expansion is accompanied with local distortion of the initial straight path of ribs and cross-sections, an upgrade of the theoretical compression moduli, Eqs.(2,6), provides the following values: 92 GPa in helical ribs, 116 GPa in hoop ribs, and 123 GPa in reinforced helical ribs.

5. Axial compression of single units

Longitudinal stiffness of helical ribs can be readily evaluated from axial compression of single triangular units. These units include two intersecting helical ribs and two hoop ribs forming a closed cell (Figure 6). Such approach was firstly adopted in analytical and experimental study of lattice structure for future Japanese launchers [3], showing that the lateral buckling mode was the critical failure mechanism for the cell. In our case, lateral buckling did not occur because the triangular unit was sufficiently thick. Actually, the scope of this test was just to focus on compressive stiffness and strength properties of ribs. However, we remark that the system of cells is normally more prone to lateral buckling than the single unit, in which the edge effects are more pronounced.

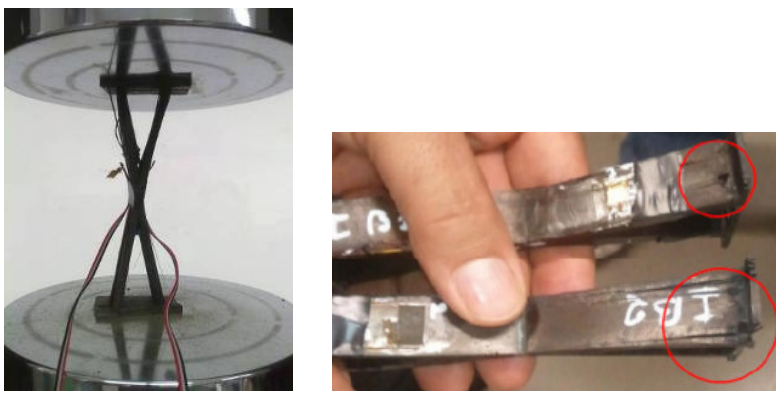

Figure 6. Example of axial compression on single unit cell and a typical failure mode (longitudinal splitting).

We also remark that the use of such sub-element is in principle analogous to the single helical ribs, because the state of stress is essentially longitudinal along the ribs. In addition, it is rather representative of the lattice structure because the overall cell is being stressed, including helical ribs, hoop ribs and the nodal region, in a rather close correspondence with the real situation. From the other side, in case of single helical ribs, at least one problem of duplication of specimens is raised: specimens in which the gauge length is occupied by the nodal region, and specimens in which the gauge length is not occupied by the nodal region. The use of this sub-element greatly reduces time for specimen preparation. In fact, the need to cut the single ribs with the proper length and to provide tabs to fit with standard test fixtures is just avoided. The only preparation for the unit cell involves some surface finishing of hoop ribs which will be in direct contact with the rigid plates. The use of strain-gauges back-to-back in helical ribs to detect possible deflection is analogous to the standard test. Then, the longitudinal stiffness of helical ribs from this unit cell will be given by the following:

$$E = \frac{\Delta\sigma}{\Delta\varepsilon} = \frac{1}{A\Delta\varepsilon}\frac{\Delta P}{2\cos\varphi} \tag{7}$$

in which A represents, as earlier, the cross-sectional area of helical ribs, φ is the rib helical angle, P is the compressive applied load (cross-head) and ε is the measured strain in the rib (average value of two opposite gauges). This evaluation is applied to a liner portion of the curve. An example of the strain measurements of helical and hoop gauges for the baseline and the reinforced microstructure is plotted vs. the compressive load in Figure 7. The positive strain in hoop ribs reveals the typical strain field in lattice structures under the action of compressive load.

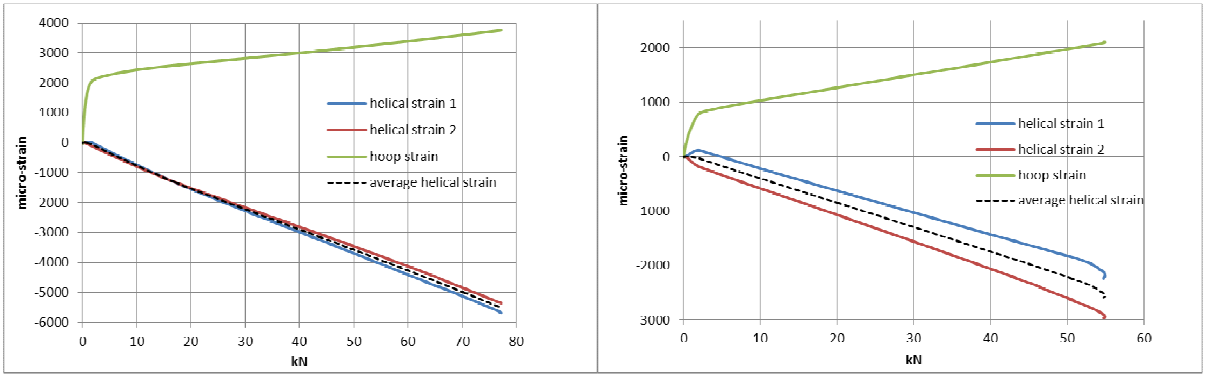

Figure 7. Axial compression of single unit: baseline ribs on the left (E = 85.6 GPa), reinforced ribs on the right (E=114 GPa).

6. Flexural stiffness and strength

The interest of a flexural stiffness test arises from the possibility to get a more accurate evaluation of the bending modulus which directly affects an important design constraint of lattice shells and panels without the skin, i.e. the lateral buckling of the system of periodic cells [4,5]. Four-point-bending tests were then conducted for the baseline and reinforced ribs (Figure 8) using in principle a standard procedure [6]. We note that, in this specific case, the geometry of the specimen was probably not optimized, but results to be a compromise in order to obtain a minimum set of samples. However, considering the linear portion of the respective bending curves, we calculate the bending modulus = 71 GPa, and the bending strength = 910 MPa, for the baseline helical ribs, whereas for reinforced helical ribs the

modulus is similar to the baseline but the strength is lower. Flexural properties did not benefit from the increased fiber fraction in the ribs (additional pieces are not continuous across the nodes).

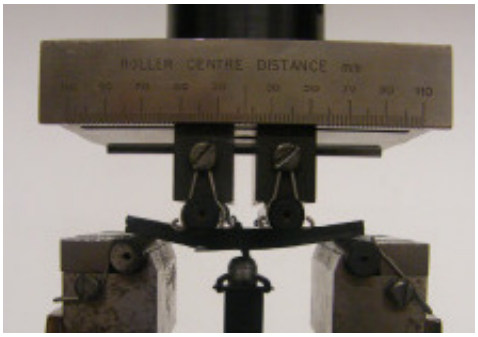

Figure 8. Example of four-point bending test of helical ribs.

7. Coefficient of thermal expansion

An evaluation of the longitudinal CTE of specimens of hoop and helical ribs extracted from the baseline microstructure [7] is shown in Figure 9. It can be seen that this coefficient changes from 0.5E-6 $°C^{-1}$ up to 1.5E-6 $°C^{-1}$. The increase of about 3 times from hoop to helical specimen can be just attributed to the different fiber volumetric fraction in such ribs, as earlier remarked. In fact, because of the higher influence of the resin on such property with respect to the longitudinal stiffness, the different fiber and resin contents both contribute to modify the CTE of respective ribs, making the overall lattice panel relatively more or less thermally stable. This tendency can be also anticipated in light of a micromechanical formulation of the CTE of a unidirectional composite lamina.

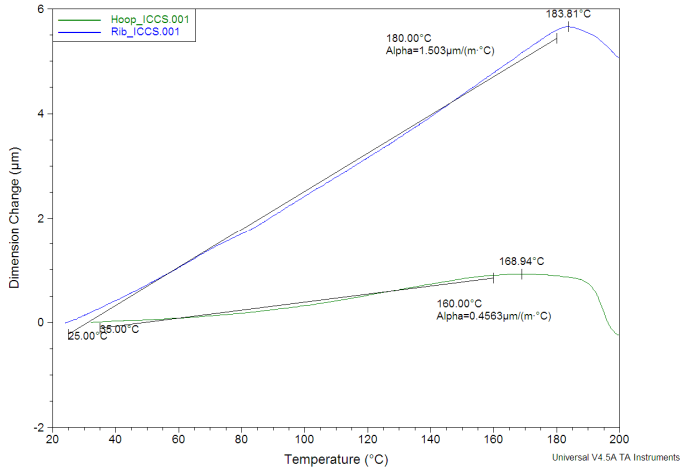

Figure 9. Example of the longitudinal CTE in hoop and helical ribs (baseline rib microstructure).

Conclusions

Manipulation of the typical fiber volumetric fraction in composite lattice structures and an innovative rubber tooling approach were suggested in this work, starting from the baseline manufacturing process represented by the dry (robotic) filament winding and resin infusion. Preliminary experimental results showed a possible trend for manufacturing to be more deeply examined in the future. In particular, the use of reinforced ribs gives the possibility to

improve the specific stiffness properties (longitudinal modulus and CTE) for application in which mechanical loads are relatively low with respect to stiffness requirements. Ideally, the initial fiber volumetric fraction, the rubber tooling, and the cure cycle should be concurrently designed in order to find the optimal compromise between stiffness and strength of ribs, also in consideration that the compaction exerted by the rubber tooling depends on the specific geometry (anisogrid cell) and is in general not homogeneous (rib distortion).

Acknowledgments

This activity was funded by the National Program for Aerospace Research within the ICCS project (Innovative Composite Cold Structure). Authors want also to thank two French Air Force cadets, namely, Meigane Burnet and Brian Barbier for their contribution in the specific activity, including the test-article manufacturing and report.

References

[1] V.V. Vasiliev, V.A. Barynin, A.F. Razin. Anisogrid composite lattice structures for – Development and aerospace applications. *Composite Structures* 94:1117-1127, 2012.

[2] G. Totaro and F. De Nicola. Recent advance on design and manufacturing of composite anisogrid structures for space launchers. *Acta Astronautica* 81:570-577, 2012.

[3] K. Terashima, T. Kamita, G. Kimura et al. Experimental and analytical study of composite lattice structure for future Japanese launchers. In *19th International Conference on Composite Materials (ICCM19)*, pages 5373-5382, 2013.

[4] G. Totaro. Local buckling modelling of isogrid and anisogrid lattice cylindrical shells with hexagonal cells. *Composite Structures* 95:403-410, 2013.

[5] G. Totaro, F. De Nicola, P. Caramuta. Local buckling modelling of anisogrid lattice structures with hexagonal cells: An experimental verification. *Composite Structures* 106:734-741, 2013.

[6] ASTM-D790-86, *Standard test methods for flexural properties of unreinforced and reinforced plastics and electrical insulating materials*.

[7] G. Totaro, G. Cosentino, F. De Nicola. Thermal modelling of anisogrid lattice structures. In *17th International Conference on Composite Structures (ICCS17)*, Porto, 2013.